View metadata, citation and similar papers at core.ac.uk
brought to you by CORE
provided by Repository of the Academy's Library

Anatomically heterogeneous populations of CB_1 cannabinoid receptor-expressing interneurons in the CA3 region of the hippocampus show homogeneous input-output characteristics

Gergely G. Szabó[1*], Orsolya I. Papp[1*], Zoltán Máté[2], Gábor Szabó[2] and Norbert Hájos[1]

[1] Lendület Laboratory of Network Neurophysiology, [2] Division of Medical Gene Technology, MTA Institute of Experimental Medicine, Hungarian Academy of Sciences, H-1450, Budapest, Hungary

*G.G.Sz., and O.I.P. contributed equally to this work.

Abbreviated title: CB1-expressing interneurons in CA3.

Number of pages: 30
Number of tables: 3
Number of figures: 8

Correspondence:

Norbert Hájos
Institute of Experimental Medicine
Hungarian Academy of Sciences
Budapest H-1450, Hungary
Phone: 36-1-2109400/387
Fax: 36-1-2109412
Email: hajos@koki.hu

Grant sponsor: National Office for Research and Technology
Grant number: OMFB-01678/2009
Grant sponsor: MTA-Hungarian Academy of Sciences
Grant number: LP2012-23/2012

Keywords: carbachol, GABAergic cell, endocannabinoids, synaptic inhibition, cholecystokinin

Abstract

A subpopulation of GABAergic cells in cortical structures expresses CB_1 cannabinoid receptors (CB_1) on their axon terminals. In order to understand the function of these interneurons in information processing, it is necessary to uncover how they are embedded into neuronal circuits. Therefore, the proportion of GABAergic terminals expressing CB_1 and the morphological and electrophysiological properties of CB_1-immunoreactive interneurons should be revealed. We investigated the ratio and the origin of CB_1-expressing inhibitory boutons in the CA3 region of the hippocampus. Using immunocytochemical techniques, we estimated that approximately 40 % of GABAergic axon terminals in different layers of CA3 also expressed CB_1. To identify the inhibitory cell types expressing CB_1 in this region, we recorded and intracellularly-labeled interneurons in hippocampal slices. CB_1-expressing interneurons showed distinct axonal arborization, and were classified as basket cells, mossy-fiber-associated cells, dendritic-layer-innervating cells or perforant-path-associated cells. In each morphological category, a substantial variability in axonal projection was observed. In contrast to the diverse morphology, the active and passive membrane properties were found to be rather similar. Using paired recordings, we found that pyramidal cells displayed large and fast unitary postsynaptic currents in response to activating basket and mossy-fiber-associated cells, while they showed slower and smaller synaptic events in pairs originating from interneurons that innervate the dendritic layer, which may be due to dendritic filtering. In addition, CB_1 activation significantly reduced the amplitude of the postsynaptic currents in each cell pair tested. Our data suggest that CB_1-expressing interneurons with different axonal projections have comparable physiological characteristics, contributing to a similar proportion of GABAergic inputs along the somato-dendritic axis of CA3 pyramidal cells.

Introduction

Cortical networks, including the hippocampus, comprise excitatory principal neurons and GABAergic inhibitory cells (Somogyi et al., 1985). Morphologically and functionally heterogeneous populations of inhibitory interneurons provide powerful control of principal cell function (Cobb et al., 1995; Miles et al., 1996) and are thus critically important for information processing (Buzsáki and Chrobak, 1995; Buzsaki and Moser, 2013). GABAergic cells in cortical circuits that express type 1 cannabinoid receptors (CB_1) at their axon terminals form a unique group of local circuit neurons (Katona et al., 1999; Marsicano and Lutz, 1999). The inhibitory synaptic output of these interneurons can be effectively suppressed by activating CB_1 (Hajos et al., 2000; Wilson and Nicoll, 2001) over a time period during which plastic changes at excitatory synapses may take place (Carlson et al., 2002). Thus, these interneurons are in a position to substantially affect learning processes at the cellular level (Puighermanal et al., 2009).

In the hippocampus, the neuropeptide cholecystokinin (CCK), 5-HT3 serotonergic receptors (Morales and Bloom, 1997), nicotinic receptors containing alpha7 subunits (Freedman et al., 1993) and M3 muscarinic receptors (Cea-del Rio et al., 2010) have been consistently identified in CB_1-expressing interneurons (Freund and Katona, 2007). In spite of the uniform expression of several receptor proteins and CCK, these interneurons show diverse morphological properties. In the CA1 region of the hippocampus, CB_1 was shown to be present at boutons of inhibitory cells targeting different subcellular regions of pyramidal cells: basket cells that innervate the perisomatic region of the pyramidal cells, Schaffer collateral-associated cells that project mainly to the stratum radiatum and also perforant-path-associated cells projecting to the stratum lacunosum-moleculare (Katona et al., 1999; Hajos et al., 2000; Cope et al., 2002; Klausberger et al., 2005). Thus, the outputs of CB_1-expressing interneurons are distributed along the somato-dendritic axis of pyramidal cells in accordance with the main afferent pathways of the CA1 region. In contrast to the variability in axonal projection, CB_1-expressing interneurons in CA1 display rather similar properties in their synaptic output and firing behavior during distinct network activities *in vivo* (Klausberger et al., 2005; Daw et al., 2009).

In the CA3 region, an area proposed to have distinct roles in memory function compared to CA1 (Buzsaki and Moser, 2013), CB_1-expressing interneurons with diverse axonal arbors fire differently during theta and gamma oscillations (Lasztoczi et al., 2011). This finding suggests different roles for these CA3 interneuron types in hippocampal

operation. However, very little is known about the electrophysiological characteristics and features of the output synapses of CB_1-expressing interneurons, which may influence their contribution to network activity.

Here, we found that approximately 40% of GABAergic terminals expressed CB_1 in the different layers of the CA3 hippocampal region. In spite of anatomical variability in the axon arbors, interneurons immunolabeled for CB_1 were homogenous in their active and passive membrane characteristics, as well as in the properties of their output synapses. Our results indicate that different CB_1-expressing interneurons contribute to the GABAergic innervation of distinct CA3 pyramidal cell surface domains to a similar extent.

Materials and Methods

Animals and Slice Preparation. All experiments were carried out in accordance with the Hungarian Act of Animal Care and Experimentation (1998, XXVIII, section 243/1998, renewed in 22.1/360/3/2011), and with the guidelines of the institutional ethical code. Interneurons for electrophysiological recordings were sampled in slices prepared from wild type mice (CD1 or C57Bl/6J strains) or from transgenic mice expressing enhanced green fluorescent protein (eGFP) controlled by the glutamate-decarboxylase 65 promoter (GAD65, (Lopez-Bendito et al., 2004)). Some interneurons for morphological studies were intracellularly labeled in slices prepared from mice expressing red fluorescent protein (DsRed) under the control of the cholecystokinin promoter (BAC-CCK-DsRED, (Mate et al., 2013)). Mice of both sexes (postnatal day 15–23) were deeply anaesthetized with isoflurane and decapitated. The brain was quickly removed and placed into ice-cold cutting solution containing (in mM): 205 sucrose, 2.5 KCl, 1.25 NaH_2PO_4, 5 $MgCl_2$, 0.5 $CaCl_2$, 26 $NaHCO_3$, and 10 glucose. The cutting solution was bubbled with 95% O_2 /5% CO_2 (carbogen gas) for at least half an hour before use. Horizontal hippocampal slices (300 μm thick) were prepared using a Leica VT 1000S or a VT1200S microtome (Leica, Nussloch, Germany), and kept in an interface-type holding chamber at room temperature for at least 60 min before recording in standard ACSF with the composition of (in mM) 126 NaCl, 2.5 KCl, 1.25 NaH_2PO_4, 2 $MgCl_2$, 2 $CaCl_2$, 26 $NaHCO_3$, and 10 glucose. Solutions were prepared with ultrapure water and bubbled with carbogen gas.

CB_1 content of GABAergic boutons. To reveal the ratio of GABAergic boutons expressing CB_1, some slices prepared for electrophysiological recordings from wild type mice were immediately fixed overnight in 4% paraformaldehyde in 0.1 M phosphate buffer (PB; pH 7.4). After fixation, slices were washed with 0.1 M PB several times, embedded in 1% agar, and re-sectioned to 40 μm thickness. The sections were then blocked in 10% Normal Donkey Serum (NDS,Vector Laboratories, Burlingame, CA) made up in Tris-buffered saline (TBS, pH 7.4) followed by incubation in a mixture of primary antisera of rabbit anti-CB_1 (1:1000, Cayman Chemical Company, Ann Arbor, MI), goat anti-GAD65/67 (1:1000, Frontier Institute Co. Ltd., Sapporo, Japan), and guinea pig anti-VGAT (1:1000, Frontier Institute Co. Ltd., Sapporo, Japan) diluted in Tris-Buffered Saline (TBS) containing 1% NDS and 0.1% Triton X-100 for three days at 4ºC. Following several washes in TBS, the sections were incubated in a mixture of secondary antisera of Alexa 594-conjugated donkey anti-rabbit

(1:500, Invitrogen, Carlsbad, CA), Alexa 488-conjugated donkey anti-goat (1:500, Invitrogen), and Alexa 647-conjugated donkey anti-guinea pig (1:500, Invitrogen) diluted in TBS for 2 hours to visualize the CB_1-expressing boutons in red, the GABAergic axon endings in green and in far-red, respectively. Following several washes in TBS, sections were mounted on glass slides in Vectashield (Vector Laboratories). Coverslips were sealed in nail polish. Images were taken using an AxioImager Z1 microscope (Zeiss, Germany) with 40x objective (NA=0.75), or an A1R confocal laser scanning microscope (Nikon Europe, Amsterdam, The Netherlands) using a 60× (NA = 1.4) objective.

For quantitative analysis, high magnification (60 nm/pixel) *z*-stack images were taken at 60x magnification from the upper 3 μm of the slices (*z*-step was 130 nm) using a Nikon A1R microscope. To improve the quality of the images, deconvolution was carried out with the Huygens Professional program (Hilversum, The Netherlands). For counting the colocalization of CB_1, GAD65/67 and VGAT staining, one stack from the upper 1 μm was chosen, where the antibodies penetrated properly. From a 61.44 μm^2 area chosen randomly, the putative immunopositive boutons were marked in one of the labelings with the NIS-Elements Software (Nikon), and their positivity was investigated on the same image for the other two stainings. When the overlap of the three antibody staining could not be unequivocally determined in the boutons based on the confocal stack used for the evaluation of the colocalization, the neighboring stacks were used to inspect the colocalization.

Electrophysiological recordings. Slices were transferred to a submerged type recording chamber. The flow rate was 2-3 ml/min. Experiments were performed at room temperature under visual guidance using an Olympus microscope (BX61WI, Olympus Corp., Tokyo, Japan). Fluorescence of eGFP- and DsRed-containing cells was excited by a monochromator at 488 nm and at 550 nm wavelength, respectively, and the resulting fluorescence was visualized with a CCD camera (TILL photonics, Gräfelfing, Germany). Whole-cell patch-clamp recordings were made using a Multiclamp 700B amplifier (Molecular Devices), filtered at 2 kHz, digitized at 5 kHz with a PCI-6024E board (National Instruments, Austin, TX), recorded with an in-house data acquisition and stimulus software (Stimulog, courtesy of Prof. Zoltán Nusser, Institute of Experimental Medicine, Hungarian Academy of Sciences). Patch pipettes were pulled from borosilicate glass capillaries with inner filaments to have a resistance of 3-6 MΩ (1.5 mm O.D.; 1.12 mm I.D., Hilgenberg GmbH, Malsfeld, Germany). To obtain recordings from CB_1-expressing interneurons in CA3, cells were selected by the eGFP content (in slices prepared from GAD65-eGFP mice), by the DsRed expression (in

slices prepared from BAC-CCK-DsRed mice), or by the soma size and by on-line investigation of their firing characteristics using gradually increasing hyper- and depolarizing current steps (in slices prepared from wild type mice). The CB_1 immunostaining in the CA3 region of the hippocampus was similar between wild-type mice and mice from both transgenic lines (Supplementary figure 1). Due to this, we combined the analysis of CB_1-expressing interneuron properties across all strains. Additionally, all cells measured in slices originating from wild type mice were tested for CB_1 positivity *post hoc* with immunostaining. Data from two cells that could not be identified successfully as CB_1-expressing were not included in this study. In slices prepared from GAD65-eGFP mice, we preferentially selected eGFP-positive cells possessing large somata that corresponded to the interneurons expressing CB_1 (Figure 2; (Wierenga et al., 2010)). The intrapipette solution used for the interneurons contained (in mM) 110 K-gluconate, 4 NaCl, 2 Mg-ATP, 40 HEPES, 0.3 GTP, 0.2% biocytin, adjusted to pH 7.3 using KOH, osmolarity was 290 mOsm/l. After break-in, we tested the voltage responses to a series of hyperpolarizing and depolarizing square current pulses of 800 ms duration and amplitudes between -100 and 100 pA at 10 pA step intervals, then up to 300 pA at 50 pA step intervals and finally up to 600 pA at 100 pA step intervals from a holding potential of -65 mV in each cell. Using these voltage responses, we characterized any active and passive membrane properties of CB_1-expressing interneurons with an in-house analysis software SPIN 1.0.1 (courtesy of Prof. Zoltán Nusser), and a custom-made program written in MATLAB (for details, see Tables 1 and 2 and (Antal et al., 2006; Papp et al., 2013). Rheobase was defined as the minimum current step at which the cell fired at least 3 action potentials. The maximal current step was the highest current injection generating firing without distortion. The decay time constant of IPSCs was obtained by fitting a single exponential decay to the descending phase of synaptic events. Using slice preparations, single cell properties were examined in 38 interneurons from wild-type and 35 interneurons from GAD65-eGFP mice. There were no significant differences ($p>0.1$) in these properties between groups, therefore these results from both mouse lines were pooled.

In paired recordings, the presynaptic cell was a CB_1-expressing interneuron and the postsynaptic cell was a pyramidal cell. The intrapipette solution used for the postsynaptic cell contained (in mM) 80 CsCl, 60 Cs-gluconate, 1 $MgCl_2$, 2 Mg-ATP, 3 NaCl, 10 HEPES, and 5 QX-314 (2(triethylamino)- *N*-(2,6-dimethylphenyl) acetamine), adjusted to pH 7.3 with CsOH, and the osmolarity was 295 mOsm/l. Presynaptic interneurons were held in current clamp mode at a membrane potential of -65 mV, and stimulated by brief current pulses (1.5 ms, 1-2 nA) to evoke action potentials. Pyramidal cells were clamped at the holding potential

of -65 mV. Series resistance (between 5-20 MΩ) was frequently monitored and compensated by 65%. Cells where the series resistance has changed more than 25% during recording were discarded from further analysis. To investigate the dynamics of the transmitter release and the magnitude of the asynchronous release, we calculated the average of unitary inhibitory postsynaptic current (IPSC) amplitudes in response to ten action potentials at 30 Hz evoked in the presynaptic cell. These trains of action potentials were evoked at 0.05 Hz during each recording (Figure 7).

Post hoc **anatomical identification of interneurons**. After recording, slices were fixed overnight in 4% paraformaldehyde in 0.1 M PB (pH 7.4). Following fixation, slices were washed with 0.1 M PB several times. Biocytin-filled cells from GAD65-eGFP mice were visualized with Alexa 488-conjugated streptavidin (Alexa 488, 1:3000, Invitrogen), while filled interneurons from wild type or BAC-CCK-DsRed mice were visualized with Cy3-conjugated streptavidin (1:1000; Sigma-Aldrich). It was possible to visualize the axons of the interneurons despite the fact that the conjugated fluorophore was the same color already expressed by the transgenic animals because the fluorophore conjugated to streptavidin generates a much stronger signal in axon terminals compared to the genetically encoded fluorescence. If axon collaterals of the recorded cells could be seen, then slices were embedded in 1% agar and re-sectioned to 40 μm thickness. The sections were then blocked in NGS (10%, Vector Laboratories) made up in TBS (pH 7.4) followed by incubation in rabbit anti-CB_1 (Cayman Chemical Company, Ann Arbor, MI) diluted 1:1000 in TBS containing 2% NGS and 0.05% Triton X-100. Following several washes in TBS, CB_1 expression was visualized using Alexa 594 (goat anti-rabbit, 1:500, Invitrogen) on GAD65-eGFP mice and Alexa 488 (goat anti-rabbit, 1:500, Invitrogen) in BAC-CCK-DsRed mice. In cases of both single and double stainings, the incubations were followed by several washes in TBS. Sections were mounted on slides in Vectashield (Vector Laboratories). Images were taken using an AxioImager Z1 microscope (Zeiss, Germany) or a Nikon A1R confocal laser scanning microscope using a 60× (NA = 1.4) objective. For high magnification images, single confocal images or maximum intensity *z*-projection images were used (2-3 confocal images at 0.3-3 μm).

Subsequently, representative interneurons were further developed by immunoperoxidase reaction using Nickel-intensified Di-amino-benzidine (DAB-Ni), for morphological reconstruction. Briefly, biocytin was visualized using avidin-biotinylated horseradish peroxidase complex reaction (ABC; Vector Laboratories) with DAB-Ni as a

chromogen. After dehydration and embedding in Durcupan (Fluka), neurons were reconstructed with the aid of a drawing tube using a 40x objective. To determine the proportion of the labeled interneuron axons in various layers of the hippocampus, we scanned in drawings of axon arbors into Adobe Photoshop and quantified the pixels representing axons, normalized to the background. Coefficient of variation (CV, the standard deviation divided by the mean) of axonal distribution was calculated from the proportion of the axon collaterals in the principal layer for each cell in a given group.

Statistical analysis. In those cases, where the Shapiro-Wilk and Kolmogorov-Smirnov tests rejected the hypothesis that the data were taken from normal distributions, a non-parametric Kruskal-Wallis (KW) ANOVA or Mann-Whitney (MW) test was performed and data are presented as median and interquartile range. Otherwise, ANOVA, paired or two sample t-test was used and the results are given as mean±SEM. Pearson's chi-square tests with Bonferroni correction were used for comparison of the CB_1-expressing bouton ratios among different layers. STATISTICA 11 software (Statsoft, Inc., Tulsa, OK) or Origin 8.6 software (Northampton, MA) was used for statistical evaluations of differences.

RESULTS

A large population of GABAergic boutons expresses CB_1 in the CA3 region of the hippocampus

In order to reveal the proportion of GABAergic axon endings expressing CB_1, we visualized inhibitory boutons with an antibody developed against both isoforms of the GABA synthesizing enzyme GAD (GAD65 and GAD67) or in a separate set of experiments, with an antibody developed against the vesicular GABA transporter, VGAT and co-stained the sections in both cases with an antibody that recognizes CB_1. In the stratum pyramidale, where most axon terminals are inhibitory (Megias et al., 2001; Kaneko et al., 2002), we found that 70% of CB_1-positive axon terminals (273 out of 391 boutons from three animals) were also positive for GAD65/67 and, similarly, 78% of CB_1-expressing axon terminals (307 out of 391 boutons from three animals) were immunoreactive for VGAT. This incomplete co-localization of these two proteins defining the GABAergic phenotype of axon terminals with CB_1 was unexpected, because the antibody used to visualize CB_1 in this study labels only

inhibitory, but not excitatory boutons (Hajos et al., 2000). Therefore, we next tested the co-localization of GAD65/67 and VGAT in the boutons located in the stratum pyramidale, although a previous study showed that VGAT and GAD65/67 could be present even at the same synaptic vesicles (Jin et al., 2003) and should thus label the same set of GABAergic terminals. In contrast to this obvious prediction, we observed that there was a large, but not complete overlap between these two markers for GABAergic phenotype under our conditions (88% of VGAT-immunolabeled boutons (389 from 440 boutons) showed GAD65/67 immunoreactivity; 87% of GAD65/67-immunoreactive boutons (349 from 403 boutons) were VGAT immunopositive, tested in the stratum pyramidale in three animals). Therefore, we chose to label inhibitory terminals by a mixture of antibodies developed against VGAT and GAD65/67 to maximize the number of visualized GABAergic boutons.

Under our conditions, confirming our previous data (Hajos et al., 2000), the anti-CB_1 antibody labeled mainly, if not exclusively GABAergic terminals, because the vast majority of CB_1-immunpositive boutons was found to be immunoreactive for GAD65/67 and/or VGAT in all layers of CA3 (81% of CB_1-immunoreactive boutons (277 out of 341) in the stratum oriens; 86% (336 out of 391) in the stratum pyramidale; 90% (383 out of 427) in the stratum lucidum; 94% (290 out of 307) in the stratum radiatum; 91% (349 out of 384) in the stratum lacunosum-moleculare were immunopositive for GAD65/67 or VGAT, calculated from three animals). Conversely, we found that approximately 40% of all inhibitory axon terminals labeled for GAD65/67/VGAT were immunopositive for CB_1 irrespective of the layer in CA3 (Figure 1, Table 1). The only exception was the stratum pyramidale, in which layer the percentage of CB_1-expressing GABAergic boutons was 50%, a proportion that was significantly higher compared to that found in strata lucidum, radiatum and lacunosum-moleculare, but not in stratum oriens ($P<0.01$, Pearson's chi-square test). This surprisingly high ratio of CB_1-expressing GABAergic varicosities indicates that CB_1 can control the GABA release in a significant proportion of inhibitory axon endings in CA3.

Morphology of interneurons expressing CB_1 in CA3

In the next set of experiments, we aimed to determine the origin of the CB_1-expressing boutons in CA3. To uncover the interneuron types giving rise to this dense meshwork of axon endings immunoreactive for CB_1 in all layers of CA3, we intracellularly-labeled interneurons in hippocampal slices. CB_1-expressing interneurons were identified by immunolabeling for CB_1 in case of cells sampled in slices prepared from wild type mice (n=90), GAD65-EGFP

transgenic mice (n=40) or BAC-CCK-DsRed mice (n=5). In slices prepared from GAD65-EGFP transgenic mice green cells with large soma were preferentially targeted, which interneurons express CB_1 (n=40; Figure 2, (Wierenga et al., 2010)). After morphological identification, a total of 135 identified interneurons were included in the study.

Based on their axonal projection, CB_1-expressing interneurons in CA3 could be divided into four main groups (Figure 3). Axon collaterals of basket cells (BC, n=38) were mostly present in the pyramidal cell layer and its vicinity (Figure 4A). Mossy-fiber-associated cells (MFA cell, n=32) had their axon clouds mainly in the stratum lucidum, and gave rise to some additional collaterals in the hilus. Axon arbors of dendritic-layer-innervating cells (DLI cell, n=52) were observed prevalently in the stratum radiatum, but their axon branches could be occasionally traced into the stratum moleculare of the dentate gyrus. Perforant-path-associated cells (PPA cell, n=11) projected their axons almost exclusively into the stratum lacunosum-moleculare. Overall, these interneurons with different axon arborization patterns had comparable multipolar dendritic trees, covering several layers of the CA3. Although there was some correspondence between the location of the cell bodies of different types of CB_1-expressing interneurons and their main axonal projection, a considerable overlap between the soma locations of distinct interneuron types could be noticed. In general, BCs were sampled mainly within or near the stratum pyramidale, MFA cells in the stratum lucidum, DLI cells in the middle part of the stratum radiatum, while PPA cells were most often found at the border of strata radiatum and lacunosum-moleculare. However, in each cell category, cell bodies could be often found outside of the 'principal' location listed above, where the majority of the somata of a given cell type was identified (Figure 4). In addition to the variability in the soma location of CB_1-expressing interneuron types, there was a substantial diversity in axonal arbors within each class of cells (Figure 4). We often observed smaller or larger deviations from the 'prototypical' examples (Figure 3). To compare quantitatively the axon arbors of distinct cell types filled in slice preparations, we measured the axon length in distinct layers. While the stratum pyramidale and stratum radiatum was divided into two and three equal bins, respectively, all other layers in CA3 and in the dentate gyrus were represented as a single bin (Figure 4). Although BCs could have wide axon clouds penetrating deeply even into strata radiatum or oriens, or, in contrast, could display a narrow axon tree at the border of strata pyramidale and oriens (Figure 4A), on average the majority of the axon cloud was restricted to the stratum pyramidale (70.2±17.2 %, CV (coefficient of variation) =0.24 , n=8). While the axon arbors of MFA cells were mainly present to the stratum lucidum (43.9±14.01%, CV=0.32, n=9), their axon collaterals often innervated the closest part of the stratum

pyramidale (15.05±7.9%) and of the stratum radiatum (20.3±11.5%). In 15 out of 32 MFA cells, their axons were found to penetrate into the hilus. The most diverse axon clouds were observed in case of DLI cells. Although, on average, the axon cloud of DLI cells was mainly found in the stratum radiatum (79.6±22.3%, CV=0.28, n=6), their collaterals were observed in the stratum oriens, and occasionally also penetrated into the stratum lacunosum-moleculare. In contrast to this 'wide' axonal appearance, we also observed DLI cells with narrow axonal arborization within the stratum radiatum (Figure 4C). In 20 out of 52 DLI cells, axon collaterals were observed in the stratum moleculare of the dentate gyrus. The least variance in axon projection was noticed among PPA cells. In most of the cases, their axons were restricted to the stratum lacunosum-moleculare (83.3±8.8%, CV=0.11; n=5), but we found examples where axon collaterals of PPA cells left the stratum lacunosum-moleculare and formed a meshwork in the stratum radiatum close to the border of the stratum lacunosum-moleculare (Figure 4D). In addition to these previously identified cell types (Lasztoczi et al., 2011), we found two interneurons with their axon clouds predominantly, albeit not exclusively located in the stratum oriens (82.4% and 37.1% of the total axon, respectively, Figure 4E). A part of their axon collaterals penetrated into the strata pyramidale and lucidum.

In summary, four main types of CB_1-expressing interneurons were identified in CA3 with rather similar dendritic morphology, but we observed a large morphological diversity in their axonal projections, even among cells within each of these categories. Furthermore, two interneurons were identified, which had axon arbors mainly in the stratum oriens.

Membrane properties of CB_1-expressing interneurons

Next, we asked whether the differences in axon arborization also manifest as individual cell features. To address this question, we investigated the active and passive membrane properties of CB_1-expressing interneurons in slices prepared from wild type mice or from GAD65-EGFP transgenic mice. To this end, we injected gradually-increasing depolarizing and hyperpolarizing current steps into the interneurons using the whole-cell patch-clamp technique, and analyzed their voltage responses. We found that the majority of the examined parameters (9 out of 15) were similar in the four anatomically-distinguished cell types (Table 2). However, we found some significant differences, e.g. action potential threshold, the adaptation of action potential amplitude, and relative sag amplitude differed between groups (Table 2). It is interesting to note that, although the membrane capacitance between cell types differed (Table 2), their membrane time constants were similar, offset by input resistance

(Table 2). To compare the firing capability of distinct cell types, we plotted the firing frequency as a function of the intracellularly-injected current step amplitudes (Figure 5A). We observed that all types of CB_1-expressing interneurons responded to a given current input with similar spiking frequencies (Figure 5B).

These data show that in contrast to the large morphological variance in axon arbors of CB_1-expressing interneurons, most of their single-cell properties and firing characteristics are similar.

Features of CB_1-expressing interneuron output synapses

The possible differences in synaptic inhibition along the somato-dendritic axis of pyramidal cells can substantially impact the signal processing. Therefore, in addition to membrane properties, we aimed to compare various features of synaptic transmission at the synaptic outputs of CB_1-expressing interneurons. To this end, we performed paired recordings between CB_1-expressing interneurons and their pyramidal cell partners in the CA3 region of hippocampal slices. The probability of finding a monosynaptically coupled pair was 83% (51 pairs out of 61 trials). Due to the lack of detectable postsynaptic response in all but one dual recording from PPA cell and pyramidal cell pairs (peak amplitude, 38.5 pA; potency, 34.4 pA; 10-90% rise time, 7.66 ms, decay time constant, 14.3 ms; probability of failures, 0.1; latency, 2.85 ms, charge of asynchronous release, 899 pA*ms, the ratio of the 10^{th} and the 1^{st} uIPSC amplitude, 1.15), we focused our study on the synaptic properties of connections originating from BCs (n=20), MFA cells (n=14) and DLI cells (n=21). Unitary inhibitory postsynaptic currents (uIPSCs) in pyramidal cells were evoked by single action potentials in the presynaptic interneurons. We compared the peak amplitude (including failures), potency (excluding failures), 10-90% rise time and decay time constant. Additionally, the synaptic latency of transmission (i.e. the time between the peak of action potentials and the beginning of the uIPSC) as well as the probability of transmission failures were calculated (Figure 6, Table 3). Statistical comparison of these data revealed that the peak amplitude of the uIPSC (P<0.001, KW ANOVA), the synaptic potency (KW ANOVA; P<0.001), the 10-90% rise time (P=0.002, KW ANOVA), and the decay time constant (P=0.009, KW ANOVA) were different. Post-hoc statistical investigations showed that DLI cells differ significantly from the other two groups in their synaptic potency, 10-90% rise time and decay time constant, while the uIPSC amplitude was found to be different only between BC-pyramidal cell and DLI cell-

pyramidal cell pairs (Table 3). No difference could be detected in failure rate (P=0.56, KW ANOVA) or latency (P=0.82, KW ANOVA; Figure 6B, Table 3) among the three groups.

These results show that the properties of output synapses of BCs and MFA cells are similar, while the differences observed at synaptic contacts between DLI cells and pyramidal cells may be explained by the dendritic location of the synapses, because dendritic filtering could substantially affect the amplitude and rise time of uIPSCs recorded at the soma (Spruston et al., 1993).

Comparison of short-term plasticity and the magnitude of asynchronous release at the synapses of CB_1-expressing interneurons

In our previous study, we found that the output synapses of BCs show little, if any, short-term changes in the uIPSC amplitude evoked by a train of action potentials on average (Szabó et al., 2010). Here, we extended this investigation by testing the synaptic dynamics in other types of CB_1-expressing interneurons contacting pyramidal cells. Consistent with our previous results, we found that in BC-pyramidal cell pairs, the short-term plasticity evaluated by trains of ten action potentials evoked at 30 Hz was variable, observing depressing, facilitating or facilitating-depressing patterns, but on average there was no substantial change in the uIPSC amplitude during the train (median: 0.78, interquartile range: 0.65-1.49, n=19; Figure 7A-C). Synapses in DLI cell-pyramidal cell pairs behaved similarly (median: 0.85, interquartile range: 0.66-1.08, n=24; Figure 7A-C). In contrast, facilitation or facilitation-depression characterized the synapses in most of the MFA cell-pyramidal cell pairs on average (median: 1.11, interquartile range: 0.59-1.40, n=14; Figure 7A-C). At the population level, the short-term plasticity depicted by the ratio of the 10^{th} and the 1^{st} uIPSC amplitude during the train was distinct at synapses in MFA cell-pyramidal cell pairs compared to that observed in DLI cell-pyramidal cell pairs (P<0.05, MW test, Figure 7C). Next, we asked the question whether the differences in short-term dynamics in IPSC amplitude during a train of action potentials (Figure 7) might be explained by the variations in tonic activation of CB_1 at axon terminals (Losonczy et al., 2004). We specifically examined the BC- and MFA-pyramidal cell connections and compared the IPSC amplitudes recorded in these cell pairs before and after the bath-application of AM251. The rationale behind the comparison of the AM251 effect only for the output synapses of BCs and MFA cells was that the axonal arborizations of these GABAergic cells preferentially occupy the perisomatic region of CA3 pyramidal cells, thus, neither the electrical filtering of signals (Figure 6), nor the spatial

difference in the axon arbors (Figure 4) would substantially affect the results. The analysis revealed that the AM251 treatment similarly increased the IPSC amplitude evoked by single action potentials recorded in BC- and MFA-pyramidal cell pairs (141.9±28.8% of control, n=7, and 240.1±98.9% of control, n=4, respectively, *P*=0.258). In these experiments, AM251 wash-in caused a significant increase in IPSC amplitude in two BC- and two MFA-pyramidal cells pairs (*P*<0.05, paired t-test), but not in other pairs. At population level, this CB_1 antagonist under these recording conditions did not alter the IPSC amplitudes significantly in either groups (*P*=0.25 for BC, n=7; *P*=0.28 for MFA, n=4, paired t-test). As in the previous set of experiments (Figure 6, Table 3), the amplitude of IPSCs recorded during control period was comparable in BC-pyramidal cell pairs (248.1±51.5 pA, n=7) and in MFA-pyramidal cell pairs (260.7±97.1 pA, n=4; *P*=0.9, two sample t-test). These results suggest that the tonically active CB_1 receptors at axon terminals of interneurons that innervate the perisomatic region of CA3 pyramidal cells similarly impact the basal synaptic transmission, and thus these receptors may not be primarily responsible for the difference in short-term plasticity under our recording conditions. In summary, these data indicate that BCs and DLI cells provide a constant synaptic inhibition along the somato-dendritic axis of CA3 pyramidal cells for a period of time when activated synchronously, while MFA cells can dynamically change their inhibitory control in the mossy fiber termination zone if the spiking of MFA cells evolves during network activities.

Earlier works (Hefft and Jonas, 2005; Daw et al., 2009; Szabo et al., 2010) have described how a train of action potentials can be followed by a sustained and significant release of GABA from axon endings expressing CB_1, but this feature is less pronounced at boutons containing a Ca^{2+} binding protein parvalbumin. This prolonged synaptic inhibition followed by a spike train was named asynchronous release, which was proposed to be the result of the build-up of the intra-boutonal Ca^{2+} concentration during the spike trains that lasts for tens of milliseconds. Since we found earlier that a train of ten action potentials evoked at 30 Hz is very effective in inducing asynchronous release at synapses of CB_1-expressing BCs, we tested the ability of the output synapses of MFA and DLI cells to produce a prolonged post-train inhibition using the same protocol. We found that asynchronous release of GABA could be detected in all the tested types of CB_1-expressing interneuron-pyramidal cell pairs, but the magnitude of this prolonged inhibition was different for each interneuron type (charge in pA*ms: BC; median: 974.1, interquartile range: 712.2-2589.4, n=19; MFA; median: 2171.1, interquartile range: 691-6679.2, n=14; DLI; median: 823.7, interquartile range: 488.6-2088.1, n=24; Figure 7A, D). By comparing the IPSC charge before and after the action

potential trains, larger sustained inhibition was observed at synapses formed by MFA cells than by DLI cells (P<0.05, MW test; Figure 7D). These results show that MFA cells have the ability to impact the function of their main postsynaptic partners, the CA3 pyramidal cells, for longer period of time than BCs or DLI cells.

CB_1 activation at the output synapses of interneurons projecting onto distinct domains of CA3 pyramidal cells similarly decreases the IPSC amplitude

In order to confirm that CB_1 cannabinoid receptors detected immunocytochemically at the output synapses of investigated interneuron types are indeed functional, we tested the endocannabinoid sensitivity of these connections. The endocannabinoid release from the postsynaptic pyramidal cells was achieved by activating M1/3 muscarinic receptors. As it was previously shown, the activation of these cholinergic receptors triggers release of retrograde signaling molecules from pyramidal cells in a Ca^{2+} dependent manner, resulting in the reduction of the IPSC amplitude, which reduction could be prevented by blocking CB1 function (Fukudome et al., 2004; Makara et al., 2007; Neu et al., 2007). Using this well-established protocol to activate CB_1 at inhibitory synapses, we applied 5 μM carbachol (CCh), a cholinergic receptor agonist during paired recordings and evaluated the CCh effects at individual synaptic connections. In these experiments the average amplitude of postsynaptic responses evoked by 10 action potentials at 30 Hz was obtained (i.e. we measured the amplitude of 10 individual IPSCs evoked by a train and calculated their average) and compared before and during the drug treatment. We observed that CCh application invariantly reduced the averaged IPSC amplitude in all the connections tested (n=16). In BC-pyramidal cell pairs, the IPSC amplitudes were significantly reduced to 15.0±10.9% of control upon CCh treatment (control, 130.7±31.1 pA; in CCh, 12.5±8.5 pA, n=6, P=0.01, paired t-test). In MFA-pyramidal cell pairs, CCh suppressed the IPSC amplitude to 3.2±1.1 % of control (control, 156.4±63.2 pA; in CCh, 3.2±0.8 pA, n=4, P=0.045, paired t-test). In DLI-pyramidal cell pairs, the amplitudes of IPSCs decreased to 23.1±6.3% of control in the presence of CCh (control, 36.9±3.6 pA; in CCh, 7.7±1.7 pA, n=6, P <0.001, paired t-test)(Figure 8A-C, G). The efficacy of the depression caused by CCh did not differ among pairs grouped by interneuron type (P=0.31, ANOVA, Figure 8G).

Next, we tested whether the reduction in IPSC amplitudes upon CCh treatment was mediated via CB_1 receptor activation. To this end, the effects of CCh on IPSC amplitude were evaluated in 2 μM AM251 applied for 30-40 min before the CCh treatment. In all three types

of interneuron-pyramidal cell pairs, the pre-treatment of slices with AM251 prevented the significant suppression of IPSC amplitudes upon CCh application, indicating that this cholinergic agonist reduced the inhibitory synaptic transmission indeed via CB_1 activation (BC-pyramidal cell pairs, in AM251, 181.8±31.7 pA, in AM251+CCh, 147.4±29.4 pA, n=6, *P*=0.1; MFA-pyramidal cell pairs, in AM251, 111.2±27.7 pA, in AM251+CCh, 74.3±11.3 pA, n=3, *P*=0.11; DLI-pyramidal cell pairs, in AM251, 38.6±8.0 pA, in AM251+CCh, 33.9±7.0 pA, n=6, *P*=0.09, paired t-test, Figure 8D-G).

In the last part of these experiments, we aimed to clarify whether M1/3 muscarinic receptors were involved in CCh-induced suppression of inhibitory transmission, similarly to that observed in other brain regions (Fukudome et al., 2004; Makara et al., 2007; Neu et al., 2007). Indeed, the pre-treatment of slices in a M1/3 muscarinic receptor antagonist (10 μM pirenzepine) blocked the effect of CCh at inhibitory synapses, because no significant reduction in IPSC amplitude could be detected in paired recordings (BC-pyramidal cell pairs, in Pir, 98.8±30.8 pA, in Pir+CCh, 79.6±20.8 pA, n=5, *P*=0.17; MFA-pyramidal cell pairs, in Pir, 95.2±32.8 pA, in Pir+CCh, 79.5±25.7 pA, n=3, *P*=0.35; DLI-pyramidal cell pairs, in Pir, 35.2±9.6 pA, in Pir+CCh, 26.4±6.9 pA, n=5, *P*=0.07, paired t-test, Figure 8G).

Our data collectively suggests that the activation of M1/3 muscarinic receptors leads to endocannabinoid production and these signaling molecules can effectively suppress synaptic transmission at the output synapses of CB_1-expressing interneurons in the CA3 region.

Discussion

One of the main findings of our study is that approximately 40% of GABAergic boutons in each layer of CA3 were found to be immunoreactive for CB_1. However, we cannot rule out the possibility that a small proportion of GABAergic boutons were not labeled, even when using antibodies recognizing the two key proteins of the inhibitory phenotype. The large proportion of inhibitory boutons expressing CB_1 seems to be surprising in the light of previous immunocytochemical findings, where the ratio of distinct classes of GABAergic cells was estimated by counting the immunoreactive cell bodies. These estimates proposed that CB_1/CCK-expressing GABAergic cells form approximately 10-15 % of all GABAergic cells in the hippocampus (Kosaka et al., 1985; Jinno and Kosaka, 2006). The apparent discrepancy between our study and previous estimations strengthens the idea that distinct types of inhibitory cells could give rise to a substantially different number of varicosities (for

review see (Bezaire and Soltesz, 2013). An alternative explanation, which does not rule out the previous scenario, might be that the detection of CCK or CB_1 levels at some somata can be below the threshold of the immunostaining, whereas at axon endings CB_1 can be readily visualized. This latter possibility is in accordance with the *in situ* data, showing that mRNA of CB_1 could be detected in approximately 40% of GABAergic cell bodies in the hippocampus (Marsicano and Lutz, 1999). In summary, our results suggest that in the CA3, a significant proportion of GABAergic boutons expresses CB_1, making it possible to control GABA release by endogenous and exogenous agonists of CB_1 at a substantial fraction of inhibitory axon endings.

The second important observation of this study is that under our recording conditions the large morphological variability of CB_1-expressing interneurons is accompanied by similar electrophysiological properties regarding both the single-cell characteristics and the features of synaptic transmission. The morphological diversity of axon arbors of both CB_1/CCK-expressing basket cells and dendritic-layer-innervating cells has already been acknowledged (Cope et al., 2002; Klausberger et al., 2005; Lasztoczi et al., 2011; Tricoire et al., 2011). In contrast to the large anatomical variability, the single-cell properties of distinct morphological types of CB_1/CCK-expressing interneurons in CA3 were found to be rather similar, except some features where we revealed significant differences, similarly to that found in CA1 (Cea-del Rio et al., 2011). One of the differences was the slower decaying phase of IPSCs at the output synapses of DLI cells in comparison with BCs or MFA cells. The reason for this could be two-fold. First, dendritic filtering might play a substantial role in shaping the IPSC kinetics recorded at the soma (Spruston et al., 1993; Maccaferri et al., 2000). Second, the subunit composition of $GABA_A$ receptors at the output synapses of CB_1-expressing interneurons targeting the distinct surface of pyramidal cells could also be distinct, potentially contributing to the slower IPSCs with dendritic origin (Pearce, 1993; Nyiri et al., 2001). Overall, both the similarities and differences in the investigated properties were comparable to that found in the case of CB_1/CCK-expressing interneurons recorded in CA1 (Cope et al., 2002; Lee et al., 2010; Cea-del Rio et al., 2011; Iball and Ali, 2011) or in the neocortex (Galarreta et al., 2008; De-May and Ali, 2013). Similarly to the previous studies obtained in CA1 (Daw et al., 2009; Lee et al., 2010), we observed that uIPSCs evoked by BCs or MFA cells were faster and larger than those evoked by DLI cells, as may be expected from the differences in synaptic location along the somato-dendritic axis of postsynaptic pyramidal cells. This observation may imply that uIPSCs originating from dendritic synapses can have comparable size and kinetics locally, at the site of their origin, to those events that derive from perisomatic

synapses. Hence, the inhibitory potency of synapses given rise to by distinct types of CB_1-expressing interneurons might be alike locally. Moreover, we found that both the short-term plasticity of the synapses and the ability of synapses to induce asynchronous transmitter release upon a train of action potentials in BC - and DLI -pyramidal cell pairs were similar, in agreement with such observations in CA1 (Daw et al., 2009). However, the synapses formed by MFA cells were different in these features, because the dynamics of uIPSCs in MFA - pyramidal cell pairs showed facilitation-depression in general, and these GABAergic synapses could release more transmitter molecules asynchronously than those axon terminals derived from DLI cells. However, this difference in the charge following the action potential trains might be partially contaminated by excitatory postsynaptic currents if GABA from MFA cell output synapses is not taken up by transporter molecules (Booker et al., 2013), and may spill over to mossy terminals evoking glutamate release upon $GABA_A$ receptor activation (Ruiz et al., 2010).

In addition to interneurons with large cell bodies that express CB_1 in GAD65-EGFP mice, small EGFP-expressing cells were also observed. These neurons lacked CB_1 expression at their somata and, therefore, could correspond to distinct types of hippocampal GABAergic cells. A recent study demonstrated that in this transgenic mouse line neuropeptide Y (NPY), vasoactive intestinal polypeptide (VIP) and the Ca^{2+} binding protein calretinin could be found in EGFP-expressing interneurons in addition to CCK in the CA1 region (Wierenga et al., 2010). NPY-, VIP- and calretinin-containing interneurons have relatively small cell bodies (Gulyas et al., 1992; Acsády et al., 1996; Acsady et al., 1997), therefore, it is safe to assume that EGFP-positive, but CB_1-immunonegative interneurons observed in CA3 belonged to these neurochemically diverse cell types, as in CA1.

Perisomatic region-targeting interneurons (including BCs and MFA cells) and dendrite-targeting interneurons (including DLI cells and PPA cells) may fulfill distinct functions in neuronal computation (Miles et al., 1996), and therefore coordinating their activity should be important during different network states (Lovett-Barron et al., 2012). CB_1-expressing interneurons projecting to the perisomatic region or dendritic layers of pyramidal cells were found to have largely similar electrophysiological properties, therefore the question arises whether their activity can be coordinated by the same extra- or intra-hippocampal afferents. To achieve simultaneous activity of all CB_1/CCK-expressing interneurons, which would then provide a uniform inhibitory input along the complete somato-dendritic axis of CA3 pyramidal cells, a common input should excite them. Indeed, afferents from the median raphe nucleus could powerfully drive the firing of the interneurons expressing CCK or

calbindin (a calcium-binding protein that is often present in CB_1/CCK-expressing cells innervating the dendrites of pyramidal cells (Freund et al., 1990; Marsicano and Lutz, 1999; Papp et al., 1999; Varga et al., 2009)). Furthermore, cholinergic input from the medial septum may also excite CB_1/CCK-expressing interneuron, although on a longer time scale (Szabo et al., 2010; Cea-del Rio et al., 2011). Thus, at least two subcortical inputs can provide the necessary excitation for simultaneous firing of the interneurons innervating the distinct compartments of pyramidal cells. During sleep, however, when e.g. the impact of the subcortical afferents on circuit operation is less pronounced (Kaifosh et al., 2013), the inhibitory function of BCs and dendrite-innervating interneurons expressing CB_1 can be separated. In fact, it was observed that two interneuron types immunoreactive for CB_1 spiked at the different phases of the theta rhythm in anesthetized rats (Lasztoczi et al., 2011), implying that inhibition of the perisomatic and dendritic regions of pyramidal cells can alternate in time. The third possibility is that all CB_1-expressing cells could be temporarily and simultaneously silenced, relieving pyramidal cells from this significant source of inhibition. In fact, GABAergic input from the medial septum, which synapses on CB_1/CCK-expressing interneurons in the hippocampus (Gulyás et al., 1990; Papp et al., 1999), can effectively inhibit the spiking of interneurons (Tóth et al., 1997; Manseau et al., 2008), providing the basis for removing cannabinoid-sensitive synaptic inhibition from pyramidal cells. In addition to extrahippocampal afferents, operation of local circuitries may also differentially reduce the inhibitory potency of CB_1-expressing interneurons forming synapses with the different parts of pyramidal cells. For instance, endocannabinoids released upon activation of metabotropic glutamate receptors (mGlu) completely blocked GABA release from the axon endings of CB_1-positive BCs, while synaptic transmission at synapses of dendrite-targeting interneurons expressing CB_1 was found to be only partially reduced (Lee et al., 2010). This finding may imply differential control of inhibition during high network activities, when a large population of pyramidal cells fire synchronously and release enough glutamate to activate the perisynaptically-located type 1 and/or 5 mGlu (e.g. during sharp wave-ripple oscillations, or epileptic discharges, (Buzsáki et al., 1992; Bragin et al., 1997)). In this scenario, the synaptic inhibition originating from CB_1-expressing perisomatic BC terminals can collapse, whilst dendritic inhibition may still function, helping to transmit information from the hippocampus into the downstream areas by allowing pyramidal cell spiking (Cobb et al., 1995; Chrobak and Buzsáki, 1996; Miles et al., 1996).

In summary, the morphologically distinct types of CB_1/CCK-expressing interneurons giving rise to a large proportion of inhibitory synapses in the CA3 region of the hippocampus

can inhibit the somatic and dendritic domains of pyramidal cells with similar efficacy. These interneurons alternate the impact of their inhibition between the distinct functional domains of pyramidal cells in time, or temporarily relieve pyramidal neurons from synaptic inhibition, depending on the network state controlled by subcortical afferents, or by intrinsic network operation. Thus, the profound morphological diversity accompanied by similar electrophysiological characteristics of CB_1/CCK-expressing interneurons may support their different operation in hippocampal networks that are precisely controlled by network states.

Acknowledgements: The authors are grateful to Erzsébet Gregori for her excellent technical assistance, and to Beáta Németh, Károly Simon and Richárd Kozma for drawing some of the cells. The authors acknowledge help of László Barna, the Nikon Microscopy Center at Institute of Experimental Medicine, Nikon Austria GmbH, and Auro-Science Consulting, Ltd., for kindly providing microscopy support. The authors declare no conflict of interest.

Reference list

Acsády L, Arabadzisz D, Freund TF (1996) Correlated morphological and neurochemical features identify different subsets of vasoactive intestinal polypeptide-immunoreactive interneurons in rat hippocampus. Neuroscience 73:299-315.

Acsady L, Katona I, Gulyas AI, Shigemoto R, Freund TF (1997) Immunostaining for substance P receptor labels GABAergic cells with distinct termination patterns in the hippocampus. The Journal of comparative neurology 378:320-336.

Antal M, Eyre M, Finklea B, Nusser Z (2006) External tufted cells in the main olfactory bulb form two distinct subpopulations. The European journal of neuroscience 24:1124-1136.

Bezaire MJ, Soltesz I (2013) Quantitative assessment of CA1 local circuits: Knowledge base for interneuron-pyramidal cell connectivity. Hippocampus 23:751-785.

Booker SA, Gross A, Althof D, Shigemoto R, Bettler B, Frotscher M, Hearing M, Wickman K, Watanabe M, Kulik A, Vida I (2013) Differential GABAB-receptor-mediated effects in perisomatic- and dendrite-targeting parvalbumin interneurons. The Journal of neuroscience : the official journal of the Society for Neuroscience 33:7961-7974.

Bragin A, Csicsvari J, Penttonen M, Buzsaki G (1997) Epileptic afterdischarge in the hippocampal-entorhinal system: current source density and unit studies. Neuroscience 76:1187-1203.

Buzsáki G, Chrobak JJ (1995) Temporal structure in spatially organized neuronal ensembles: a role for interneuronal networks. Curr Opinion Neurobiol 5:504-510.

Buzsáki G, Horvath Z, Urioste R, Hetke J, Wise K (1992) High-frequency network oscillation in the hippocampus. Science 256:1025-1027.

Buzsaki G, Moser EI (2013) Memory, navigation and theta rhythm in the hippocampal-entorhinal system. Nat Neurosci 16:130-138.

Carlson G, Wang Y, Alger BE (2002) Endocannabinoids facilitate the induction of LTP in the hippocampus. Nat Neurosci 5:723-724.

Cea-del Rio CA, Lawrence JJ, Erdelyi F, Szabo G, McBain CJ (2011) Cholinergic modulation amplifies the intrinsic oscillatory properties of CA1 hippocampal cholecystokinin-positive interneurons. J Physiol 589:609-627.

Cea-del Rio CA, Lawrence JJ, Tricoire L, Erdelyi F, Szabo G, McBain CJ (2010) M3 muscarinic acetylcholine receptor expression confers differential cholinergic modulation to neurochemically distinct hippocampal basket cell subtypes. The Journal of neuroscience : the official journal of the Society for Neuroscience 30:6011-6024.

Chrobak JJ, Buzsáki G (1996) High-frequency oscillations in the output networks of the hippocampal-entorhinal axis of the freely behaving rat. J Neurosci 16:3056-3066.

Cobb SR, Buhl EH, Halasy K, Paulsen O, Somogyi P (1995) Synchronization of neuronal activity in hippocampus by individual GABAergic interneurons. Nature 378:75-78.

Cope DW, Maccaferri G, Marton LF, Roberts JD, Cobden PM, Somogyi P (2002) Cholecystokinin-immunopositive basket and Schaffer collateral-associated interneurones target different domains of pyramidal cells in the CA1 area of the rat hippocampus. Neuroscience 109:63-80.

Daw MI, Tricoire L, Erdelyi F, Szabo G, McBain CJ (2009) Asynchronous transmitter release from cholecystokinin-containing inhibitory interneurons is widespread and target-cell independent. The Journal of neuroscience : the official journal of the Society for Neuroscience 29:11112-11122.

De-May CL, Ali AB (2013) Cell type-specific regulation of inhibition via cannabinoid type 1 receptors in rat neocortex. Journal of neurophysiology 109:216-224.

Freedman R, Wetmore C, Stromberg I, Leonard S, Olson L (1993) alpha-bungarotoxin binding to hippocampal interneurons - immunocytochemical characterization and effects on growth factor expression. Journal of Neuroscience 13:1965-1975.

Freund TF, Gulyas AI, Acsady L, Gorcs T, Toth K (1990) Serotonergic control of the hippocampus via local inhibitory interneurons. Proc Natl Acad Sci U S A 87:8501-8505.

Freund TF, Katona I (2007) Perisomatic inhibition. Neuron 56:33-42.

Fukudome Y, Ohno-Shosaku T, Matsui M, Omori Y, Fukaya M, Tsubokawa H, Taketo MM, Watanabe M, Manabe T, Kano M (2004) Two distinct classes of muscarinic action on hippocampal inhibitory synapses: M2-mediated direct suppression and M1/M3-mediated indirect suppression through endocannabinoid signalling. Eur J Neurosci 19:2682-2692.

Galarreta M, Erdelyi F, Szabo G, Hestrin S (2008) Cannabinoid sensitivity and synaptic properties of 2 GABAergic networks in the neocortex. Cerebral cortex 18:2296-2305.

Gulyás AI, Gorcs TJ, Freund TF (1990) Innervation of different peptide-containing neurons in the hippocampus by GABAergic septal afferents. Neuroscience 37:31-44.

Gulyas AI, Miettinen R, Jacobowitz DM, Freund TF (1992) Calretinin is present in non-pyramidal cells of the rat hippocampus--I. A new type of neuron specifically associated with the mossy fibre system. Neuroscience 48:1-27.

Hajos N, Katona I, Naiem SS, MacKie K, Ledent C, Mody I, Freund TF (2000) Cannabinoids inhibit hippocampal GABAergic transmission and network oscillations. Eur J Neurosci 12:3239-3249.

Hefft S, Jonas P (2005) Asynchronous GABA release generates long-lasting inhibition at a hippocampal interneuron-principal neuron synapse. Nat Neurosci 8:1319-1328.

Iball J, Ali AB (2011) Endocannabinoid Release Modulates Electrical Coupling between CCK Cells Connected via Chemical and Electrical Synapses in CA1. Front Neural Circuits 5:17.

Jin H, Wu H, Osterhaus G, Wei J, Davis K, Sha D, Floor E, Hsu CC, Kopke RD, Wu JY (2003) Demonstration of functional coupling between gamma -aminobutyric acid (GABA) synthesis and vesicular GABA transport into synaptic vesicles. Proc Natl Acad Sci U S A 100:4293-4298.

Jinno S, Kosaka T (2006) Cellular architecture of the mouse hippocampus: a quantitative aspect of chemically defined GABAergic neurons with stereology. Neurosci Res 56:229-245.

Kaifosh P, Lovett-Barron M, Turi GF, Reardon TR, Losonczy A (2013) Septo-hippocampal GABAergic signaling across multiple modalities in awake mice. Nat Neurosci 16:1182-1184.

Kaneko T, Fujiyama F, Hioki H (2002) Immunohistochemical localization of candidates for vesicular glutamate transporters in the rat brain. The Journal of comparative neurology 444:39-62.

Katona I, Sperlagh B, Sik A, Kafalvi A, Vizi ES, Mackie K, Freund TF (1999) Presynaptically located CB1 cannabinoid receptors regulate GABA release from axon terminals of specific hippocampal interneurons. J Neurosci 19:4544-4558.

Klausberger T, Marton LF, O'Neill J, Huck JH, Dalezios Y, Fuentealba P, Suen WY, Papp E, Kaneko T, Watanabe M, Csicsvari J, Somogyi P (2005) Complementary roles of cholecystokinin- and parvalbumin-expressing GABAergic neurons in hippocampal network oscillations. The Journal of neuroscience : the official journal of the Society for Neuroscience 25:9782-9793.

Kosaka T, Kosaka K, Tateishi K, Hamaoka Y, Yanaihara N, Wu JY, Hama K (1985) GABAergic neurons containing CCK-8-like and/or VIP-like immunoreactivities in the rat hippocampus and dentate gyrus. The Journal of comparative neurology 239:420-430.

Lasztoczi B, Tukker JJ, Somogyi P, Klausberger T (2011) Terminal field and firing selectivity of cholecystokinin-expressing interneurons in the hippocampal CA3 area. The Journal of neuroscience : the official journal of the Society for Neuroscience 31:18073-18093.

Lee SH, Foldy C, Soltesz I (2010) Distinct endocannabinoid control of GABA release at perisomatic and dendritic synapses in the hippocampus. The Journal of neuroscience : the official journal of the Society for Neuroscience 30:7993-8000.

Lopez-Bendito G, Sturgess K, Erdelyi F, Szabo G, Molnar Z, Paulsen O (2004) Preferential origin and layer destination of GAD65-GFP cortical interneurons. Cereb Cortex 14:1122-1133.

Losonczy A, Biro AA, Nusser Z (2004) Persistently active cannabinoid receptors mute a subpopulation of hippocampal interneurons. Proc Natl Acad Sci U S A 101:1362-1367.

Lovett-Barron M, Turi GF, Kaifosh P, Lee PH, Bolze F, Sun XH, Nicoud JF, Zemelman BV, Sternson SM, Losonczy A (2012) Regulation of neuronal input transformations by tunable dendritic inhibition. Nat Neurosci

Maccaferri G, Roberts JD, Szucs P, Cottingham CA, Somogyi P (2000) Cell surface domain specific postsynaptic currents evoked by identified GABAergic neurones in rat hippocampus in vitro. J Physiol 524 Pt 1:91-116.

Makara JK, Katona I, Nyiri G, Nemeth B, Ledent C, Watanabe M, de Vente J, Freund TF, Hajos N (2007) Involvement of nitric oxide in depolarization-induced suppression of inhibition in hippocampal pyramidal cells during activation of cholinergic receptors. The Journal of neuroscience 27:10211-10222.

Manseau F, Goutagny R, Danik M, Williams S (2008) The hippocamposeptal pathway generates rhythmic firing of GABAergic neurons in the medial septum and diagonal bands: an investigation using a complete septohippocampal preparation in vitro. J Neurosci 28:4096-4107.

Marsicano G, Lutz B (1999) Expression of the cannabinoid receptor CB1 in distinct neuronal subpopulations in the adult mouse forebrain. The European journal of neuroscience 11:4213-4225.

Mate Z, Poles MZ, Szabo G, Bagyanszki M, Talapka P, Fekete E, Bodi N (2013) Spatiotemporal expression pattern of DsRedT3/CCK gene construct during postnatal development of myenteric plexus in transgenic mice. Cell Tissue Res 352:199-206.

Megias M, Emri Z, Freund TF, Gulyas AI (2001) Total number and distribution of inhibitory and excitatory synapses on hippocampal CA1 pyramidal cells. Neuroscience 102:527-540.

Miles R, Toth K, Gulyás AI, Hajos N, Freund TF (1996) Differences between somatic and dendritic inhibition in the hippocampus. Neuron 16:815-823.

Morales M, Bloom FE (1997) The 5-HT3 receptor is present in different subpopulations of GABAergic neurons in the rat telencephalon. J Neurosci 17:3157-3167.

Neu A, Foldy C, Soltesz I (2007) Postsynaptic origin of CB1-dependent tonic inhibition of GABA release at cholecystokinin-positive basket cell to pyramidal cell synapses in the CA1 region of the rat hippocampus. J Physiol 578:233-247.

Nyiri G, Freund TF, Somogyi P (2001) Input-dependent synaptic targeting of alpha(2)-subunit-containing GABA(A) receptors in synapses of hippocampal pyramidal cells of the rat. Eur J Neurosci 13:428-442.

Papp EC, Hájos N, Acsády L, Freund TF (1999) Medial septal and median raphe innervation of vasoactive intestinal polzpeptideücontaining interneurons in the hippocampus. Neuroscience in press:

Papp OI, Karlocai MR, Toth IE, Freund TF, Hajos N (2013) Different input and output properties characterize parvalbumin-positive basket and Axo-axonic cells in the hippocampal CA3 subfield. Hippocampus

Pearce RA (1993) Physiological evidence for 2 distinct GABA(a) responses in rat hippocampus. Neuron 10:189-200.

Puighermanal E, Marsicano G, Busquets-Garcia A, Lutz B, Maldonado R, Ozaita A (2009) Cannabinoid modulation of hippocampal long-term memory is mediated by mTOR signaling. Nat Neurosci 12:1152-1158.

Somogyi P, Hodgson AJ, Chubb IW, Penke B, Erdei A (1985) Antisera to gamma-aminobutyric acid. II. Immunocytochemical application to the central nervous system. J Histochem Cytochem 33:240-248.

Spruston N, Jaffe DB, Williams SH, Johnston D (1993) Voltage- and space-clamp errors associated with the measurement of electrotonically remote synaptic events. J Neurophysiol 70:781-802.

Szabo GG, Holderith N, Gulyas AI, Freund TF, Hajos N (2010) Distinct synaptic properties of perisomatic inhibitory cell types and their different modulation by cholinergic receptor activation in the CA3 region of the mouse hippocampus. Eur J Neurosci 31:2234-2246.

Tóth K, Freund TF, Miles R (1997) Disinhibition of rat hippocampal pyramidal cells by GABAergic afferents from the septum. J Physiol (Lond) 500:463-474.

Tricoire L, Pelkey KA, Erkkila BE, Jeffries BW, Yuan X, McBain CJ (2011) A blueprint for the spatiotemporal origins of mouse hippocampal interneuron diversity. The Journal of neuroscience : the official journal of the Society for Neuroscience 31:10948-10970.

Varga V, Losonczy A, Zemelman BV, Borhegyi Z, Nyiri G, Domonkos A, Hangya B, Holderith N, Magee JC, Freund TF (2009) Fast synaptic subcortical control of hippocampal circuits. Science 326:449-453.

Wierenga CJ, Mullner FE, Rinke I, Keck T, Stein V, Bonhoeffer T (2010) Molecular and electrophysiological characterization of GFP-expressing CA1 interneurons in GAD65-GFP mice. PloS one 5:e15915.

Wilson RI, Nicoll RA (2001) Endogenous cannabinoids mediate retrograde signalling at hippocampal synapses. Nature 410:588-592.

Table 1. Percentage of GABAergic varicosities immunoreactive for CB_1 in different strata in CA3. The results were obtained in three mice. Individual counts are indicated in each row for a given stratum.

Layer	Number of GABAergic boutons	Number of CB_1 expressing GABAergic boutons	Percentage of GABAergic boutons expressing CB_1	Average percentage from three mice (%)
str. oriens	150	62	41	42±5.6
	150	55	37	
	300	146	48	
str. pyramidale	195	101	52	**50±2.6***
	282	144	51	
	300	142	47	
str. lucidum	220	96	44	40±3.5
	266	100	38	
	256	97	38	
str. radiatum	200	82	41	39.7±3.2
	271	113	42	
	228	83	36	
str. lac.-moleculare	215	73	34	36.3±2.5
	214	83	39	
	250	90	36	

*CB_1-expressing GABAergic boutons were found in significantly higher proportion in stratum pyramidale compared with strata lucidum, radiatum or lacunosum-moleculare (P<0.01).

Table 2. Electrophysiological properties of CB_1-expressing interneurons.

	BC (n=14)	**MFA** (n=16)	**DLI** (n=26)	**PPA** (n=11)	P values (KW ANOVA)
Rheobase (pA)	175 (80-300)	100 (80-150)	150 (68-200)	150 (150-200)	0.257
AP threshold (mV)	**-36.4 (-40.2 - -33.4)**	**-41.1 (-43.6 - -37.9)**	**-37.6 (-40.8 - -32.4)**	**-35.8 (-38.3 - -33.3)**	**0.036**
AHP amplitude (mV)	10.75 (8.58-15.6)	14.65 (8.95-15.53)	12.4 (10.23-15.63)	13.7 (9.4-15.8)	0.794
AHP 25% decay	21.9 (3.45-56.75)	4.4 (2.4-20.8)	16.3 (3.15-36.55)	4.4 (2.8-13.2)	0.177
AHP 50% decay	33 (11.6-83.2)	22.6 (4.7-42.9)	26.8 (5.9-58.9)	10.6 (6.3-27.8)	0.391
AHP 75% decay	44.9 (16.9-98.7)	37.9 (9.2-61.8)	36.7 (11.3-75.9)	22.6 (13.3-42.2)	0.321
AP half width (ms)	**1.2 (1-1.4)**	**1 (1-.12)**	**1.2 (1.15-1.6)**	**1.3 (1-1.6)**	**0.039**
Maximal spike frequency (Hz)	40 (31-43)	38 (28-45)	31 (26-43)	41.3 (30-53)	0.323
Accommodation ratio	3.7 (2.9-4.8)	4.1 (3.4-4.9)	3.6 (3.1-4.3)	4.2 (3.1-4.9)	0.501
Ratio of AP amplitude adaptation	**0.89 (0.82-0.98)**	**0.66 (0.59-0.79)**	**0.76 (0.65-0.84)**	**0.69 (0.6-0.76)**	**$9.49*10^{-4}$**
	BC (n=14)	**MFA** (n=13)	**DLI** (n=19)	**PPA** (n=10)	P values (KW ANOVA)
Input resistance (MΩ)	130 (71-174)	182 (145-207)	191 (150-217)	198 (89-244)	0.083
Membrane time constant (ms)	17.8 (11.6-22.8)	19 (16.1-21.8)	19.3 (16.4-22.1)	22 (15.1-25.8)	0.382
Membrane capacitance (nF)	**0.132 (0.114-0.190)**	**0.105 (0.088-0.119)**	**0.109 (0.096-0.131)**	**0.109 (0.105-0.177)**	**0.036**
Relative sag amplitude	**0.43 (0.27-0.81)**	**0.23 (0.19-0.42)**	**0.19 (0.04-0.30)**	**0.44 (0.31-0.90)**	**0.004**
Delay of sag minimum	**95.8 (56.9-119.1)**	**106.4 (96-128.6)**	**137.7 (96.7-200.4)**	**107.9 (83-157.6)**	**0.049**

Data are given as median and interquartile range in parenthesis. The results of the *post hoc* statistical comparison with Mann-Whitney test are *AP threshold (mV):* BC vs. MFA: 0.025, MFA vs. DLI: 0.021, MFA vs. PPA: 0.015; *AP half width (ms):* MFA vs. DLI: 0.01, MFA vs. PPA: 0.041; *Ratio of AP amplitude adaptation:* BC vs. MFA: $1.98x10^{-4}$, BC vs. DLI: 0.003, BC vs. PPA: 0.005; *Membrane capacitance (nF):* BC vs. MFA: 0.011, BC vs. DLI: 0.035; *Relative sag amplitude:* BC vs. MFA: 0.018, BC vs. DLI: 0.003, DLI vs. PPA: 0.018 , *Delay of sag minimum:* BC vs. DLI: 0.01

Table 3. Summary of unitary IPSC properties.

	BC	N	**MFA**	n	**DLI**	n
Peak amplitude (pA)	114.6 (75.8-183.8)	20	68.9 (36.9-162.1)	14	**45.6 (35.5-58.2)**	21
Synaptic potency (pA)	142.8 (105.7-203.1)	20	97.8 (58.4-180.1)	14	**57.5 (49.3-76.8)**	21
Rise time (10-90%, ms)	1.49 (0.88-2.16)	19	1.72 (1.08-2.85)	14	**2.84 (2.07-4.41)**	16
Decay time const. (ms)	12.85 (7.39-9.56)	20	12.1 (10.73-13.5)	13	**18.63 (12.2-24.15)**	21
Probability of failures	0.108 (0.037- 0.175)	20	0.297 (0.025-0.4)	14	0.14 (0.05-0.28)	21
Latency (ms)	2.19 (1.89-2.98)	19	2.26 (2.02-3.09)	14	2.33 (1.78-3.09)	21

Data are given as median and interquartile range in parenthesis. The results of the post hoc statistical comparison with Mann-Whitney test are: *Peak amplitude (pA):* DLI vs. BC, $p<0.001$; DLI vs. MFA, $p=0.07$; *Synaptic potency (pA)*: DLI vs. BC, $p<0.001$; DLI vs. MFA, $p=0.015$; *Rise time (10-90%, ms):* DLI vs. BC, $p<0.001$; DLI vs. MFA, $p=0.018$; *Decay time constant (ms):* DLI vs. BC, $p=0.0102$; DLI vs. MFA, $p=0.011$.

Figure legends

Figure 1. Immunopositivity for CB_1 can be detected in a large proportion of GABAergic axon terminals in the CA3 region of the hippocampus. A, Micrograph taken at low magnification of the staining of GABAergic terminals (shown in green) and CB_1 (shown in red) in the CA3 hippocampal region. s.o., stratum oriens; s.p., stratum pyramidale; s.l., stratum lucidum; s.r., stratum radiatum; s.lm., stratum lacunosum-moleculare. Yellow boxes illustrate the area and the localization of the higher magnification pictures shown in B-G. Scale bar, 20 µm. B, E; GABAergic axon endings were visualized with a mixture of antibodies raised against GAD65/67 (panGAD) and VGAT (for illustration, both proteins are shown in green). C, F; Numerous boutons are immunostained with an antibody that recognizes mostly, if not exclusively, CB_1 present at inhibitory terminals (red). D, G; A significant fraction of GABAergic axon terminals are immunoreactive for CB_1 (white arrows). Open arrows show GABAergic boutons without visible staining against CB_1. Confocal images are taken from a single plane using a Nikon A1R microscope. Asterisks in B-D label cell bodies in the stratum pyramidale. Scale bars, 5 µm.

Figure 2. EGFP-positive cells with a large diameter in the CA3 region of the hippocampus in GAD65-EGFP mice express CB_1. A, B, Micrographs taken at a lower magnification from sections immunostained for CB_1 (red). Orange arrows show the cell bodies of large EGFP/CB_1-positive cells, while open green arrows point onto small EGFP-positive cells lacking CB_1. Scale bars, 20 µm. s.l., stratum lucidum; s.p. stratum pyramidale. A_{1-3} and B_{1-3}. Micrographs with a higher magnification are taken from the same cells as in A and B. Endogenous EGFP signal in these sections has not needed any further amplification, while CB_1 was visualized with a secondary antibody conjugated with Alexa 594. Scale bars, 10 µm. Insert in A_1: based on the diameter of somata (measured the shortest diameter), EGFP-positive cells form two distinct groups. EGFP-positive cells with a soma diameter larger than 10 µm (orange open bars) were immunoreactive for CB_1, while EGFP-positive cells with smaller soma diameter (green bars) had no detectable immunolabeling. White bars show the distribution of the soma diameters of recorded and intracellularly labeled interneurons. Note that the distribution of soma diameter for recorded interneurons and the CB_1-immunostained EGFP-positive cells overlaps.

Figure 3. Interneurons with different axonal arborization express CB_1 at their axon terminals in CA3. Four typical CB_1-expressing interneurons can be distinguished, basket cells, mossy-fiber-associated cells, dendritic-layer-innervating cells, and perforant-path-associated cells. In the camera lucida reconstructions of these neuron types, the cell bodies and the dendrites are shown in black, while the axon collaterals are in red (scale bars, 50 μm). For each example, voltage responses to depolarizing (300 pA) and hyperpolarizing current steps (from -10 to -100 pA in increments of 10 pA) are indicated (calibrations, 20 mV, 100 ms). In each case, CB_1 expression was confirmed in their axon collaterals intracellularly labeled with biocytin (scale bars, 1 μm). s.lm., stratum lacunosum-moleculare; s.r., stratum radiatum; s.l., stratum lucidum; s.p., stratum pyramidale; s.o., stratum oriens; s.m., stratum moleculare; s.g., stratum granulosum; h., hilus.

Figure 4. Large diversity of axonal projections in each type of CB_1-expressing interneuron. Camera lucida reconstructions of interneurons from each category (dendrites, black; axon, red; scale bars, 50 μm). Histograms show the proportion of axon arbors in different hippocampal layers in each cell type. One line indicate a single cell, columns indicate the average of cells. Data are presented as mean ± SD. Note that the axon arbors of interneurons belonging to a given cell class can be restricted to a given layer, but in other cases axons could cover a substantially wider range, often penetrating into neighboring strata. Right, Distribution of cell bodies of anatomically-identified types of CB_1-expressing interneurons in CA3. Note that there is a correspondence between the soma location and cell type, but a substantial overlap between the positions of cell bodies of distinct interneuron types can be observed. s.r., stratum radiatum; s.l., stratum lucidum; s.p., stratum pyramidale; s.o., stratum oriens; s.lm., stratum lacunosum-moleculare; s.m., stratum moleculare; s.g., stratum granulosum; h., hilus.

Figure 5. The firing frequencies in the four cell types upon a given current pulse are similar. A, Voltage responses to depolarizing current steps (150 pA, 300 pA, 600 pA) delivered from -65 mV. B, Average frequency-input current relationships of four interneuron types measured from a holding potential of – 65 mV. Data are presented as mean ± SD. BC, basket cells; MFA, mossy-fiber-associated cells; DLI, dendritic-layer-innervating cells; PPA, perforant-path-associated cells.

Figure 6. Basic properties of inhibitory synaptic transmission in CB_1-expressing interneuron-pyramidal cell pairs. A, Examples obtained from paired recordings, where single action potentials were evoked in three distinct types of interneurons (top traces) and the postsynaptic currents were detected in CA3 pyramidal cells (bottom traces). Ten consecutive traces are superimposed (grey) with the average of all traces (thick grey), on which exponential fits to obtain the decay time constant are shown in black. B, Comparison of the peak amplitude, the synaptic potency, the 10-90% rise time, the failure probability, the decay time constant and the latency measured at synaptic contacts between CB_1-expressing interneurons and pyramidal cells. Bars indicate medians of means (short lines) corresponding to individual cell pairs. Asterisks indicate significant differences. For more details see Table 3.

Figure 7. Short-term plasticity and the magnitude of asynchronous release at synaptic contacts between CB_1-expressing interneurons and pyramidal cells can be distinct. A, IPSCs evoked at 30 Hz show distinct dynamics depending on the presynaptic interneuron type. Ten consecutive traces are superimposed (grey) with the average of all traces (black). Vertical lines before and after the traces indicate the time intervals where the IPSC charge was calculated from to evaluate the magnitude of asynchronous release. Examples indicate that a larger IPSC charge can be measured following the IPSC train (post-train) compared to control (pre-train) at synapses of CB_1-expressing interneurons, indicative of asynchronous neurotransmitter release. B, The averages of normalized peak amplitudes of IPSCs evoked by trains of 10 action potentials at 30 Hz show no substantial changes in short-term plasticity at basket and dendritic-layer-innervating cell synapses, while synaptic contacts of mossy-fiber-associated cells display facilitation, on average. Data points on these plots are mean ± SEM. C, Short-term plasticity at output synapses of MFA and DLI cells is distinct. D, The IPSC charge after the train is larger at output synapses of MFA cells than of DLI cells. Bars indicate medians of means (short lines) corresponding to individual cell pairs. Asterisks indicate significant differences.

Figure 8. Carbachol (CCh)-induced reduction in IPSC amplitude at the output synapses of basket cells (BC), mossy-fiber-associated (MFA) cells and dendritic-layer-innervating cells (DLI) is mediated via CB_1. Example of paired recordings, where trains of action potentials at 30 Hz were evoked in the presynaptic interneurons, while IPSCs were detected in the postsynaptic pyramidal cells under control conditions (A) and in the presence of 5 μM CCh (B). C, Changes in peak amplitudes in response to CCh application as a function of time.

Filled circles indicate the amplitude of the first IPSC in the train, open circles indicate the average of the amplitudes of the ten IPSCs in the train. Numbers 1 and 2 indicate the period where traces were taken, respectively. D, E, Representative recordings in interneuron-pyramidal cell pairs obtained in the presence of 2 μM AM251 (D) and after application of 5 μM CCh (E). F, Plot of the IPSC amplitude shows no significant change following bath application of CCh in the presence of AM251 (filled circles, amplitude of the first IPSC in the train; open circles, average amplitude of the ten IPSCs in the train). G, Summary plot of the carbachol effect in the absence or presence of AM251 or pirenzepine. All data were normalized to the control values, and are represented as percentage. The numbers of pairs recorded under different experimental conditions are shown above the columns. Asterisks indicate the significant differences ($p \leq 0.01$).

Supplementary figure 1. CB_1 staining in the CA3 region of the hippocampus from three different mouse strains. Micrographs taken from sections prepared from CD1, GAD65-eGFP and BAC-CCK-DsRED mice demonstrate similar appearance of the CB_1 staining. s.o., stratum oriens; s.p., stratum pyramidale; s.l., stratum lucidum; s.r., stratum radiatum; s.lm., stratum lacunosum-moleculare. Scale bars, 20 μm.

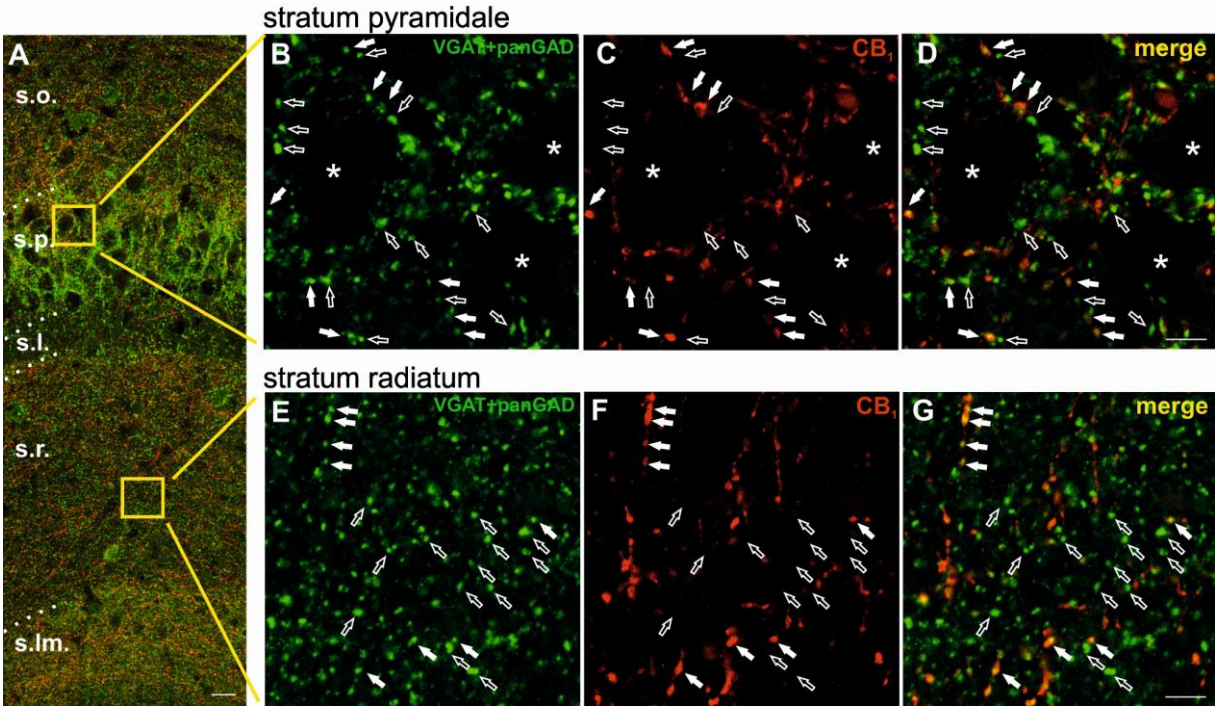
stratum pyramidale
A
s.o.
s.p.
s.l.
s.r.
s.lm.
B
VGAT+panGAD
C
CB1
D
merge
stratum radiatum
E
VGAT+panGAD
F
CB1
G
merge

fig 1

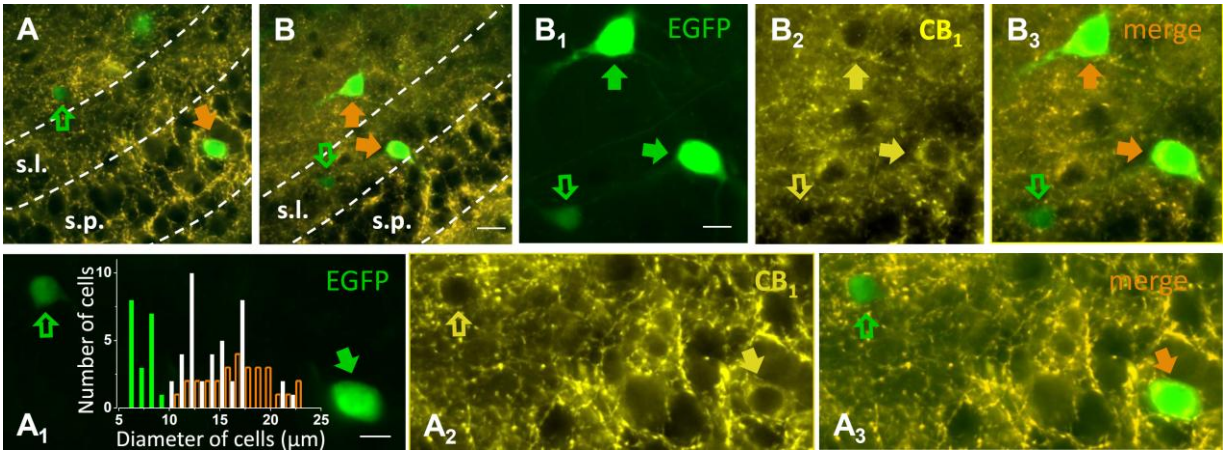
A
s.l.
s.p.
B
s.l.
s.p.
B1
EGFP
B2
CB1
B3
merge
A1
EGFP
Number of cells
10
5
0
5
10
15
20
25
Diameter of cells (µm)
A2
CB1
A3
merge

fig 2

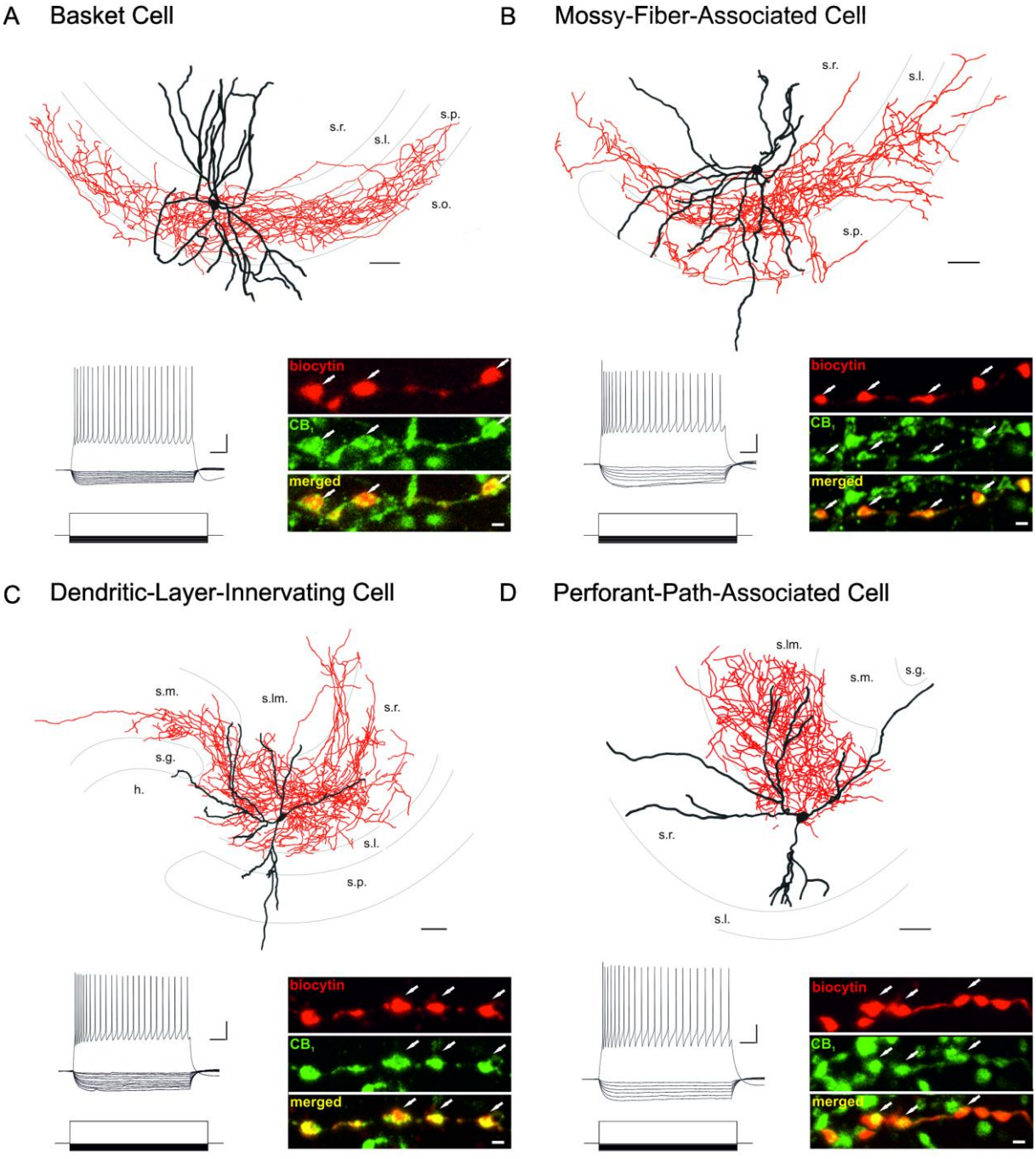
A Basket Cell
s.r.
s.l.
s.p.
s.o.
biocytin
CB1
merged
B Mossy-Fiber-Associated Cell
s.r.
s.l.
s.p.
biocytin
CB1
merged
C Dendritic-Layer-Innervating Cell
s.m.
s.lm.
s.r.
s.g.
h.
s.l.
s.p.
biocytin
CB1
merged
D Perforant-Path-Associated Cell
s.lm.
s.m.
s.g.
s.r.
s.l.
biocytin
CB1
merged

fig 3

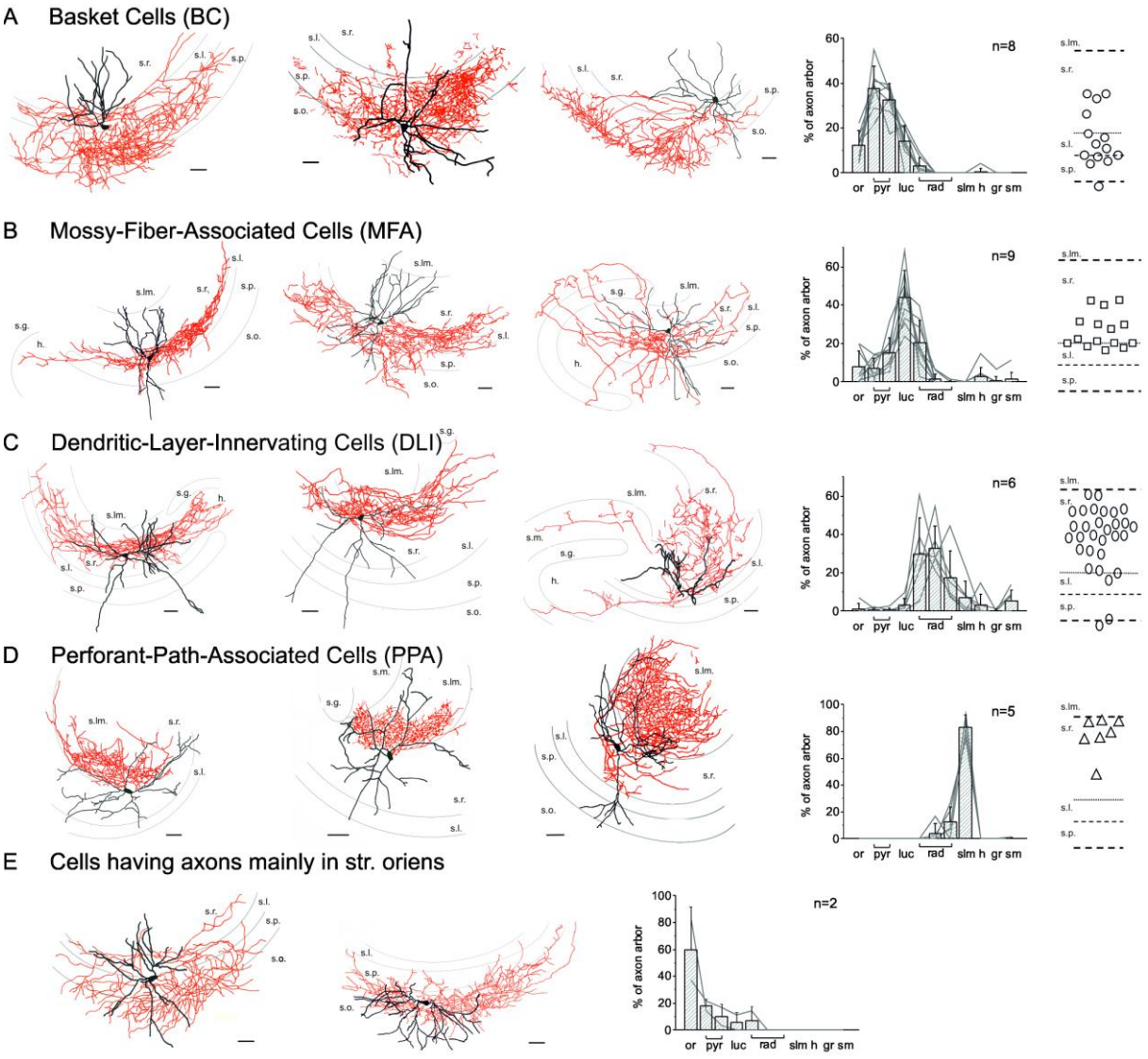
A Basket Cells (BC)
B Mossy-Fiber-Associated Cells (MFA)
C Dendritic-Layer-Innervating Cells (DLI)
D Perforant-Path-Associated Cells (PPA)
E Cells having axons mainly in str. oriens
% of axon arbor
or pyr luc rad slm h gr sm
n=8
n=9
n=6
n=5
n=2

fig 4

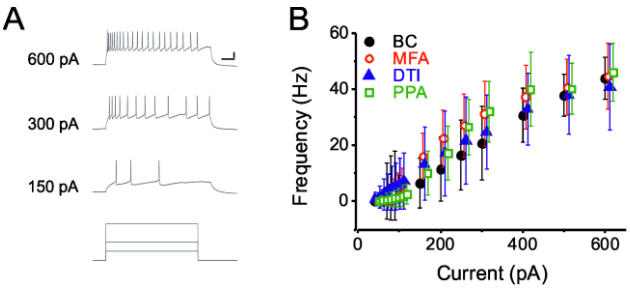
A
600 pA
300 pA
150 pA
B
BC
MFA
DTI
PPA
Frequency (Hz)
Current (pA)
0
20
40
60
0
200
400
600

fig 5

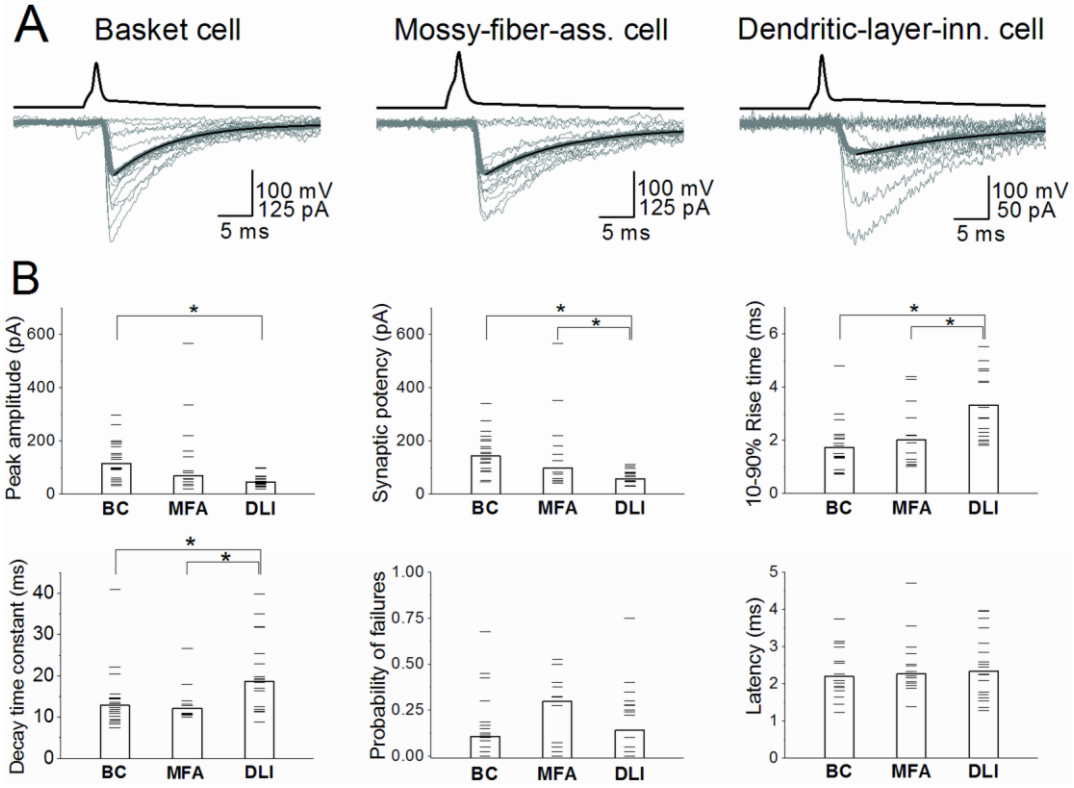
A
Basket cell
Mossy-fiber-ass. cell
Dendritic-layer-inn. cell
100 mV
125 pA
5 ms
100 mV
125 pA
5 ms
100 mV
50 pA
5 ms
B
Peak amplitude (pA)
Synaptic potency (pA)
10-90% Rise time (ms)
Decay time constant (ms)
Probability of failures
Latency (ms)
BC
MFA
DLI
*

fig 6

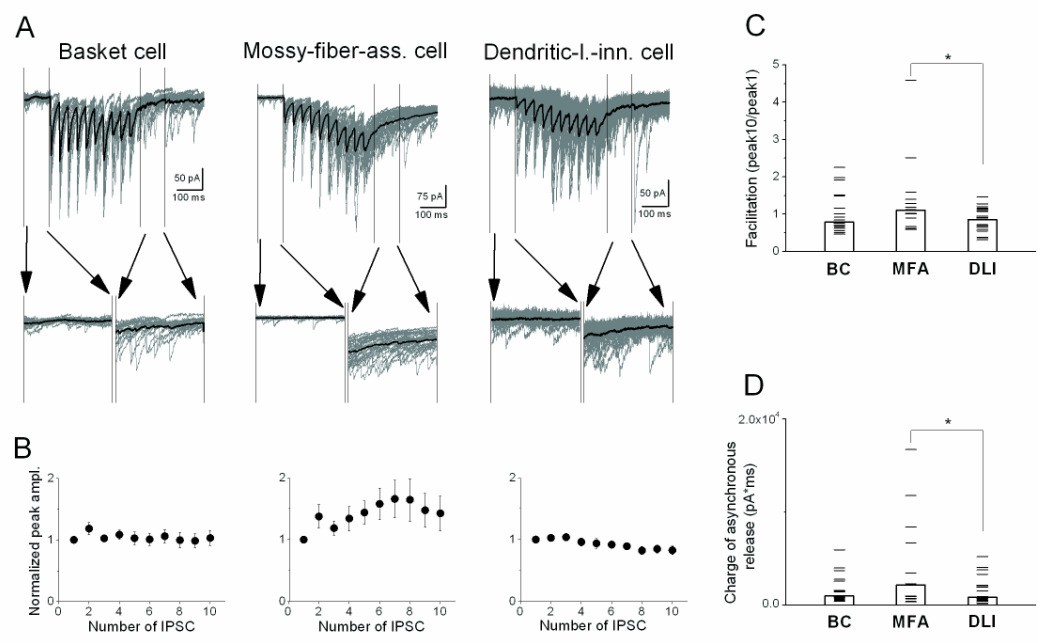
A
Basket cell
Mossy-fiber-ass. cell
Dendritic-l.-inn. cell
50 pA
100 ms
75 pA
100 ms
50 pA
100 ms
B
Normalized peak ampl.
Number of IPSC
Number of IPSC
Number of IPSC
C
Facilitation (peak10/peak1)
BC
MFA
DLI
*
D
Charge of asynchronous release (pA*ms)
2.0x10^4
0.0
BC
MFA
DLI
*

fig 7

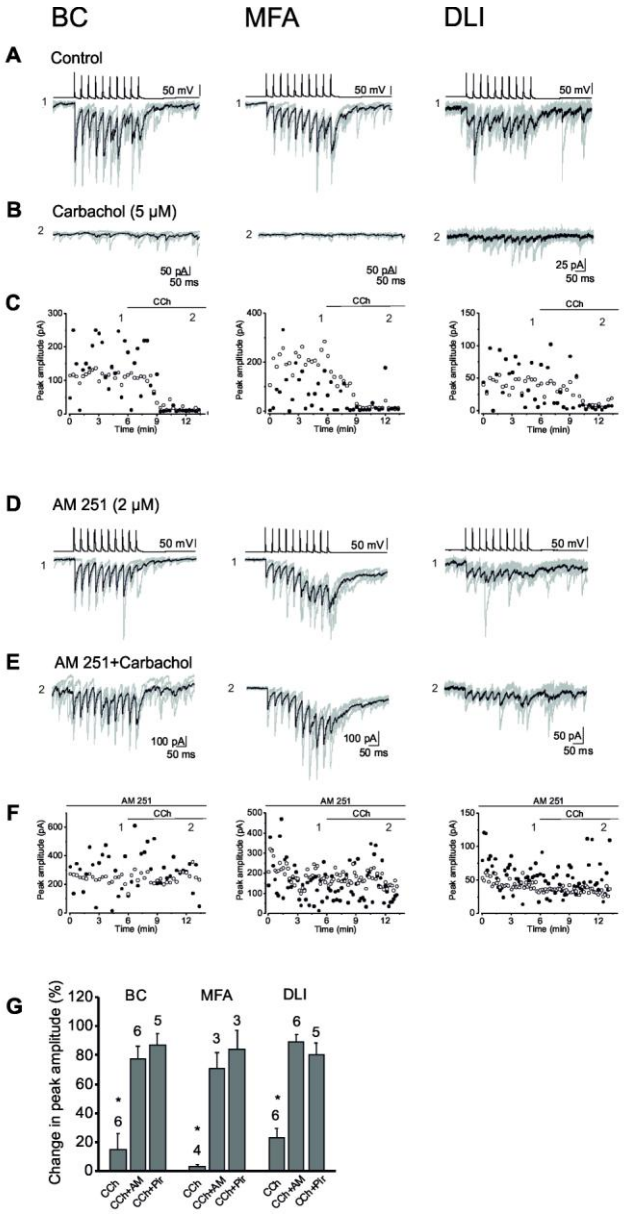
BC
MFA
DLI
A
Control
50 mV
B
Carbachol (5 µM)
50 pA
50 ms
25 pA
C
CCh
Peak amplitude (pA)
Time (min)
D
AM 251 (2 µM)
E
AM 251+Carbachol
100 pA
F
AM 251
G
Change in peak amplitude (%)
CCh
CCh+AM
CCh+Ptr

fig 8

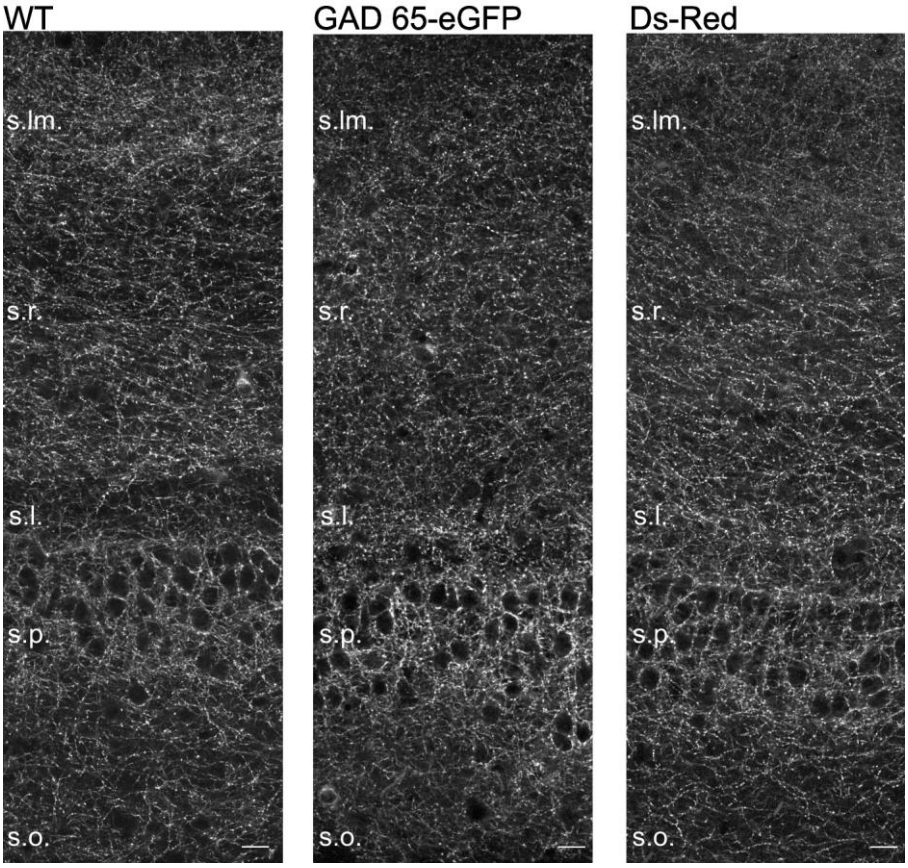

suppl. fig 1